Petroleum Science 23 (2026) 7429–7445

Contents lists available at ScienceDirect

Petroleum Science

journal homepage: www.keaipublishing.com/en/journals/petroleum-science

Original Paper

A pH-triggered delayed sodium metasilicate gel system for deep conformance control in heterogeneous reservoirs

Kun Zhang [a], Er-Dong Yao [a,*], Yi-Peng Zhong [a], Lin Tan [a], Jia-Wei Sheng [a], Li-Li Wang [b], Fu-Jian Zhou [a,**]

[a] State Key Laboratory of Petroleum Resources and Engineering, China University of Petroleum (Beijing), Beijing, 102249, China
[b] Oil & Gas Technology Research Institute, PetroChina Qinghai Oilfield Company, Dunhuang, 736202, Gansu, China

ARTICLE INFO

Article history:
Received 9 April 2026
Received in revised form
16 July 2026
Accepted 16 July 2026
Available online 21 July 2026

Edited by Yan-Hua Sun

Keywords:
Deep conformance control
Sodium silicate gel
Delayed gelation
Pore-scale characterization
Flow diversion

ABSTRACT

Conventional sodium silicate gels commonly undergo rapid and poorly controlled gelation upon direct acidification, resulting in narrow operational windows and limited deep-placement capability. To overcome these limitations, an integrated mechanism-to-application evaluation was conducted on a pH-triggered, slow-gelling silica system governed by the controlled hydrolysis of an organic ester. By systematically comparing HCl with conventional short-chain and sterically hindered ester-based latent acid generators, triethyl citrate (TEC) was identified as an effective kinetic regulator due to its steric-shielding effect. The optimized formulation—comprising 2.5 wt% sodium metasilicate, 5 wt% TEC, 0.1 wt% nano-SiO_2, and 0.1 wt% borax—exhibited a controlled gelation time of approximately 5 h at 90 °C. Dynamic light scattering, gel-strength evaluation, and microscopic characterization revealed that the system underwent hierarchical particle aggregation, ultimately evolving into a dense three-dimensional gel network with a maximum Sydansk gel strength code of H. Core flooding experiments demonstrated that the system combined high injectivity prior to gelation with robust strong plugging performance following thermal aging. In single-core tests, plugging efficiencies reached approximately 98% for the high-permeability core and 95% for the low-permeability core. In parallel dual-core flooding, the overall plugging efficiency was approximately 98%, and the flow ratio between the high- and low-permeability cores shifted from 9:1 to 3:7, and further to 1:9 following reverse flooding. These results indicate effective plugging of the dominant high-permeability channel and sustained flow diversion into the previously bypassed low-permeability zones. NMR T_2 spectra and CT scans further supported this selective placement behaviour: the gel preferentially occupied the larger pore spaces of the high-permeability core, whereas the low-permeability core exhibited only minimal gel invasion, with invasion confined to the proximal 10% of the core length. Overall, the TEC-triggered silica gel system achieves delayed gelation, deep plugging, and flow diversion, offering a promising chemical strategy for profile control in strongly heterogeneous reservoirs.

© 2026 The Authors. Publishing services by Elsevier B.V. on behalf of KeAi Communications Co. Ltd. This is an open access article under the CC BY-NC-ND license (http://creativecommons.org/licenses/by-nc-nd/4.0/).

1. Introduction

Silicate gels, a representative class of inorganic gel materials, have attracted considerable attention owing to their readily available precursors, simple preparation, and exceptional thermal and chemical stability (Katoueizadeh et al., 2020; Liu and Ott, 2020; Pham and Hatzignatiou, 2016; Quang et al., 2012). Under alkaline conditions, silicate precursors can form a three-dimensional network through progressive polycondensation, a process typically accompanied by the aggregation, growth, and crosslinking of silicate species (Brinker and Scherer, 1985; Pham and Hatzignatiou, 2016). For such systems, gel formation depends not only on precursor concentration, but also critically on system pH, acidification rate, and polycondensation kinetics (Jurinak and Summers, 1991). Accordingly, gaining precise control over both the gelation rate

* Corresponding author.
** Corresponding author.
E-mail addresses: yaoed@cup.edu.cn (E.-D. Yao), zhoufj@cup.edu.cn (F.-J. Zhou).
Peer review under the responsibility of China University of Petroleum (Beijing).

https://doi.org/10.1016/j.petsci.2026.07.031
1995-8226/© 2026 The Authors. Publishing services by Elsevier B.V. on behalf of KeAi Communications Co. Ltd. This is an open access article under the CC BY-NC-ND license (http://creativecommons.org/licenses/by-nc-nd/4.0/).

and the overall structural evolution of silicate systems remains a central challenge in this field.

Sodium metasilicate is one of the most widely used precursors for silica gel systems (Larrondo et al., 1985; Liu and Ott, 2020; Matinfar and Nychka, 2023; Wu et al., 2023). In conventional studies, strong inorganic acids such as hydrochloric acid are commonly employed to rapidly lower the system pH and induce polycondensation (Harman et al., 2021; Jesionowski, 2002; Pham and Hatzignatiou, 2016). However, although direct acid addition can effectively trigger gel formation, it also introduces pronounced kinetic control issues (Matinfar and Nychka, 2024; Sadeghnejad et al., 2022). On the one hand, the system pH is highly sensitive to the amount of added hydrochloric acid, such that even a slight change in acid concentration can cause a sharp pH shift and markedly narrow the gelation window; on the other hand, rapid acidification may lead to excessively fast local polycondensation, resulting in flocculation, precipitation, or structural heterogeneity in the gel (Katoueizadeh et al., 2020; Matinfar and Nychka, 2023). These limitations indicate that, although strong-acid triggering can accelerate gelation, it also constrains precise control over the gelation process (Hashemi et al., 2023; Zhu et al., 2021).

By contrast, latent acids provide an alternative approach to regulating the acidification of silicate systems by gradually releasing acidic species through slow hydrolysis (Hashemi et al., 2023; Ng et al., 2000). Unlike the instantaneous acidification induced by hydrochloric acid, latent acids can release acid continuously over a controlled timescale, thereby slowing the decline in system pH and extending the gelation time (Hashemi et al., 2023; Sadeghnejad et al., 2022). This controlled acid-release behaviour helps to reduce the risk of local reaction imbalance and creates favorable conditions for the gradual development of the gel network. However, the effectiveness of different latent acids is not equivalent, as it is strongly influenced by the molecular-structure-dependent hydrolysis behaviour of the acid generator (Brinker, 1988). For ester-based latent acids, the electronic effects and steric hindrance of substituents surrounding the ester group jointly determine the accessibility of reactive sites to OH^- attack, thereby influencing the hydrolysis rate, acid-release behaviour, and subsequent polycondensation kinetics of the silicate system (Katoueizadeh et al., 2020). Therefore, understanding how latent acids regulate silica gel formation from the perspective of molecular structure is of considerable importance for the design of silicate systems with tunable gelation behaviour.

Although latent acids have been employed in delayed silicate gel systems, conventional short-chain ester latent acids, such as glyceryl triacetate (GTA) and ethylene glycol diacetate (EGDA), may still exhibit relatively rapid acid release under high-temperature and strongly alkaline conditions (Katoueizadeh et al., 2020; Nasr-El-Din and Taylor, 2005). In such systems, the ester groups are more accessible to nucleophilic attack by OH^-, which can lead to a rapid pH decrease and a shortened gelation window. This behaviour limits the controllability of gel placement, particularly for deep conformance control where a sufficiently long induction period is required (Katoueizadeh et al., 2020). Therefore, it remains necessary to develop latent-acid triggers that can release acid more gradually while still effectively reducing the pH to the critical range required for sodium metasilicate polycondensation. In this work, triethyl citrate (TEC), which contains a bulky citrate backbone and three ethyl ester groups, was introduced as a sterically hindered latent acid to regulate the pH evolution and delayed gelation of sodium metasilicate systems.

On this basis, sodium metasilicate was selected as the precursor in the present study. Although hydrolysable organic esters have previously been reported as latent acid generators for silicate gelation, the structure-dependent regulation of pH evolution and gelation kinetics under high-temperature alkaline conditions remains insufficiently clarified. We first compared the effects of hydrochloric acid and several latent acids, including short-chain and sterically hindered esters, on pH evolution and gelation behaviour in order to identify suitable kinetic regulators for sodium metasilicate systems. An optimized sodium metasilicate–TEC formulation was then established, and its delayed-gelation characteristics were evaluated through gelation time, gel-strength evolution, rheological transition, thermal stability, and macroscopic appearance. Further insight into the role of TEC in regulating hydrolysis, alkalinity consumption, pH evolution, silicate polycondensation, and gel-network formation was obtained through particle-size analysis, microscopic characterization, and elemental analysis, on the basis of which a corresponding steric-hindrance-regulated gelation mechanism was proposed. Finally, the plugging performance of the silica gel system was assessed by core flooding experiments using cores with different permeabilities, together with NMR T_2 spectra and CT scanning. This study aims to elucidate the structural basis and evolution of delayed gel formation in sodium metasilicate systems from the perspective of the coupled regulation between latent-acid molecular structure and gelation kinetics, thereby establishing a structure–pH evolution–gelation–plugging correlation for controllable inorganic silica gel systems.

2. Materials and methods

2.1. Experimental materials

Anhydrous sodium metasilicate (Na_2SiO_3), corresponding to $Na_2O{\cdot}SiO_2$ with a fixed SiO_2/Na_2O molar ratio of 1.0, was utilized as the sole inorganic precursor. This low-modulus characteristic provides the highly alkaline initial environment (pH > 12) required to stabilize silicate species before acid-triggered polycondensation. To ensure consistent experimental conditions, this specific precursor was maintained across all experimental formulations. Consequently, the investigated gelation kinetics and structural evolutions were mainly associated with the pH-modulation dynamics of the acid triggers, rather than variations in the silicate precursor.

Hydrochloric acid (HCl) was used as the direct acidifying agent, and the latent acids examined included ethylene glycol diacetate (EGDA), glycerol triacetate (GTA), dibasic ester (DBE), and triethyl citrate (TEC). In addition, 0.1 wt% nano-SiO_2 and 0.1 wt% borax were incorporated into the optimized formulation to improve structural stability. Core flooding experiments were carried out using artificial cores with different permeabilities.

It should be noted that deionized water was utilized throughout this study to establish the baseline gelation kinetics of the TEC-triggered gelation. This approach minimizes the interference of divalent cations, such as Ca^{2+} and Mg^{2+}, which are commonly present in formation brines and may affect silicate aggregation or crosslinking. Although high-salinity environments are important for field applications, investigation under deionized-water conditions provides a necessary basis for clarifying the intrinsic reaction mechanism of the latent acid/sodium metasilicate system. The results should therefore be interpreted as baseline mechanistic behaviour under controlled aqueous conditions.

2.2. Preparation of gel systems

Gel systems were prepared by mixing sodium metasilicate with different acid sources at the prescribed ratios. For the HCl system, gelation was induced by direct acid addition, whereas for the latent-acid systems, the latent acid was uniformly mixed with sodium metasilicate to prepare the gel formulation. To compare the effects of different acid sources on gelation behaviour, HCl-, EGDA-, GTA-, DBE-, and TEC-based systems were prepared under the same baseline conditions, and the sodium metasilicate–TEC formulation was subsequently optimized on the basis of the screening results.

The final optimized formulation contained 0.1 wt% nano-SiO_2 and 0.1 wt% borax as auxiliary agents to synergistically enhance the gel structure. According to previous literature, trace amounts of nano-SiO_2 act as nucleation agents to improve the integrity of the initial silica network (Sheidaie et al., 2022), while borate ions provide dynamic crosslinking points to mitigate brittle fracture (Sadeghnejad et al., 2022). Since these additives primarily serve supplementary roles without altering the fundamental pH-triggered gelation pathway governed by TEC, their mechanisms were not separately investigated in this kinetic study.

The pH of each system was measured using a pH meter, and the gelation time was defined as the time required for the sample to transition from a flowable state to a stable non-flowing gel. Gelation times for systems with different acid sources were determined at room temperature and 90 °C.

2.3. Gel strength evaluation

The gelation state of the optimized system at different aging times was evaluated using the Sydansk gel-strength classification method to characterize its transition from a flowable solution to a stable gel. The gel strength code and final gelation time were determined on the basis of changes in sample appearance and flow behaviour upon vial inversion (Sydansk and Argabright, 1987).

2.4. Particle size distribution analysis

The evolution of particle size distribution in the optimized sodium metasilicate–TEC system at different reaction times was measured by dynamic light scattering (DLS) to evaluate particle aggregation and growth during gelation.

2.5. TEM and SEM characterization

Transmission electron microscopy (TEM) was used to examine the microstructure of the optimized gel system and the aggregation state of its particles, while scanning electron microscopy (SEM) was employed to characterize the microstructural features of the gel samples.

2.6. Core flooding experiments

Core flooding experiments, including both single-core and dual-core tests, were conducted to evaluate the plugging performance of the optimized gel system. All experiments were performed at 90 °C with a total injection rate of 0.3 mL/min. After core saturation, 1 pore volume (PV) of initial water flooding was applied, followed by the injection of 1 PV of the gel system. The cores were then aged under shut-in conditions for 3 d before being subjected to a further 10 PV of subsequent water flooding. Injection pressure was recorded continuously throughout the experiments to assess the plugging performance of the gel system and its ability to redirect flow under different permeability conditions.

To quantitatively evaluate the fluid blocking and plugging performance of the system, the plugging efficiency (E), residual resistance factor (RRF), and permeability reduction (PR) were calculated using the following equations:

$$E = \frac{\Delta P_{\text{after}} - \Delta P_{\text{initial}}}{\Delta P_{\text{after}}} \times 100\%$$

$$RRF = \frac{\Delta P_{\text{after}}}{\Delta P_{\text{initial}}}$$

$$PR = \left(1 - \frac{k_{\text{after}}}{k_{\text{initial}}}\right) \times 100\% = \left(1 - \frac{\Delta P_{\text{initial}}}{\Delta P_{\text{after}}}\right) \times 100\%$$

where $\Delta P_{\text{initial}}$ is the stable injection pressure differential during the initial water-flooding stage prior to gel treatment, MPa; ΔP_{after} is the stable injection pressure differential during the subsequent water-flooding stage after gel placement, MPa; k_{initial} is the initial effective permeability of the porous media before gel treatment, mD; k_{after} is the effective permeability of the residual unblocked pores after gel treatment, mD. The relationship between pressure differential and permeability was applied under identical flow-rate and fluid-viscosity conditions.

2.7. NMR and CT characterization

Low-field nuclear magnetic resonance (NMR) and computed tomography (CT) were used to characterize the distribution of pore fluids and changes in internal flow pathways before and after core flooding. By comparing the T_2 spectra and CT image features of the cores at different stages, the migration, retention, and preferential-channel plugging behaviour of the gel system were analyzed, thereby further elucidating its plugging mechanism and flooding performance.

3. Results and discussion

3.1. Effect of different acid sources on the gelation behaviour of sodium metasilicate systems

To achieve controllable regulation of gelation in sodium metasilicate systems, the effects of hydrochloric acid and different latent acids on acidification behaviour and gelation characteristics were first compared. Fig. 1 illustrates the influence of HCl concentration on the pH of the sodium metasilicate system. The pH does not decrease linearly with increasing HCl concentration; instead, it undergoes a sharp drop within a narrow concentration range, indicating that the system is highly sensitive to the amount of added hydrochloric acid. Particularly within the gelation-relevant region, even a slight change in HCl concentration causes the system pH to shift over a broad range, demonstrating that direct acidification with HCl affords only a very narrow gelation window and is therefore difficult to control precisely. Concurrently, the macroscopic appearance of the system changed markedly with pH, evolving from an initially clear and dispersed state to a turbid suspension and ultimately to a gel. This reveals that direct acid addition readily induces rapid local reactions, which is unfavourable for uniform and controlled gelation.

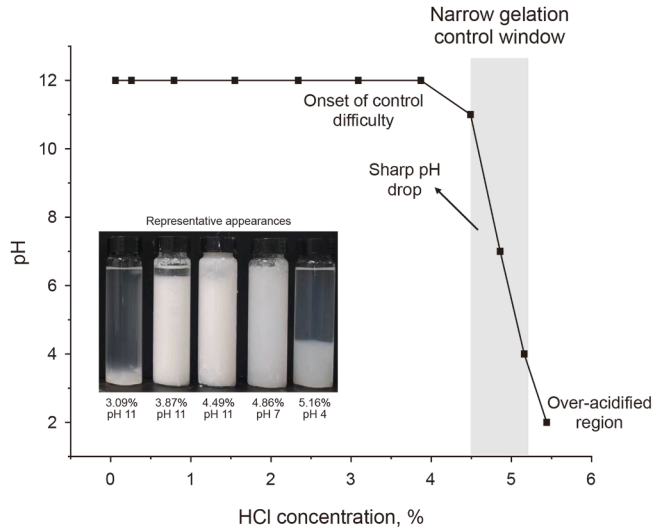


Fig. 1. Variation of pH and visual appearance of the sodium metasilicate system with HCl concentration, showing a narrow gelation control window.

Compared with direct acidification by HCl, the ester-based latent acids provided delayed gelation by gradually releasing acidic species. As shown in Fig. 2(a), HCl induced almost instantaneous gelation, whereas GTA and TEC significantly prolonged the gelation time. To further clarify the temperature response of these acid sources, the gelation times of HCl, GTA, and TEC were measured at 70, 80, and 90 °C (Fig. 2(b)). HCl triggered gelation within less than 0.1 h at all tested temperatures, confirming that direct acidification provides almost no operational window. GTA showed moderate delayed gelation, with the gelation time decreasing from 4.5 h at 70 °C to 1.0 h at 90 °C. In contrast, TEC exhibited the longest and most controllable delay, with gelation times of 15.0, 9.0, and 5.0 h at 70, 80, and 90 °C, respectively.

Based on its delayed and temperature-dependent gelation behaviour, TEC was selected as the preferred latent acid for further formulation optimization.

3.2. Gelation behaviour and formulation optimization

To elucidate the formulation–performance relationship of the TEC–sodium metasilicate system, the effects of TEC concentration and total component concentration were further evaluated (Fig. 3 and Table 1). At a fixed Na_2SiO_3 concentration of 2.5 wt%, insufficient TEC failed to trigger effective gel formation, whereas excessive TEC led to precipitation or phase separation. A stable gel system formed only within an appropriate TEC concentration range of 2.5–5.0 wt%. Furthermore, when the TEC/Na_2SiO_3 mass ratio was fixed, an excessively high absolute concentration of Na_2SiO_3 (>5.0 wt% Na_2SiO_3) induced uncontrollable flocculation and precipitation.

Based on the parametric evolution described above, the formulation containing 2.5 wt% Na_2SiO_3 + 5.0 wt% TEC was selected as the baseline formulation, primarily based on the following two engineering considerations: First, under the premise of satisfying gelation conditions, controlling the baseline silicate loading at 2.5 wt% can effectively reduce material costs. Second, because reservoir rock minerals (e.g., carbonate rocks) and ions in the formation water may consume acidic species, adopting this upper-limit proportion of TEC ensures that even in acid-consuming formation environments, the system still retains a sufficient acid-release margin to stabilize the pH at around 11.0. In practical field applications, the TEC concentration can be optimized between 2.5 and 5.0 wt% based on the site-specific formation buffering capacity. This design approach ensures both economic viability and high operational reliability, allowing engineers to tailor the formulation to the actual reservoir environment rather than relying on a fixed, high-cost standard.

Meanwhile, relevant literature indicates that nano-SiO_2 and borax, as secondary mechanical modifiers, can effectively enhance gel strength (Ahmed et al., 2017; Obut and Girgin, 2006). To minimize the influence of secondary additives on the primary TEC-triggered gelation pathway, the concentrations of nano-SiO_2 and borax were fixed at 0.1 wt% in subsequent experiments.

The formulation of 2.5 wt% Na_2SiO_3 + 5.0 wt% TEC was therefore selected as the optimized baseline system for subsequent pH-evolution and gel-strength analyses.

3.3. Gelation characteristics of the optimized sodium metasilicate–TEC system

After TEC had been identified as the most suitable latent acid, the gelation behaviour of the optimized sodium metasilicate–TEC system was further evaluated. Fig. 4(a) shows the evolution of gel strength and the corresponding macroscopic appearance of the optimized system at different times. The system did not undergo instantaneous gelation; instead, it evolved gradually from an initially flowable state into a stable, high-strength gel. As the reaction proceeded, the gel strength increased continuously,

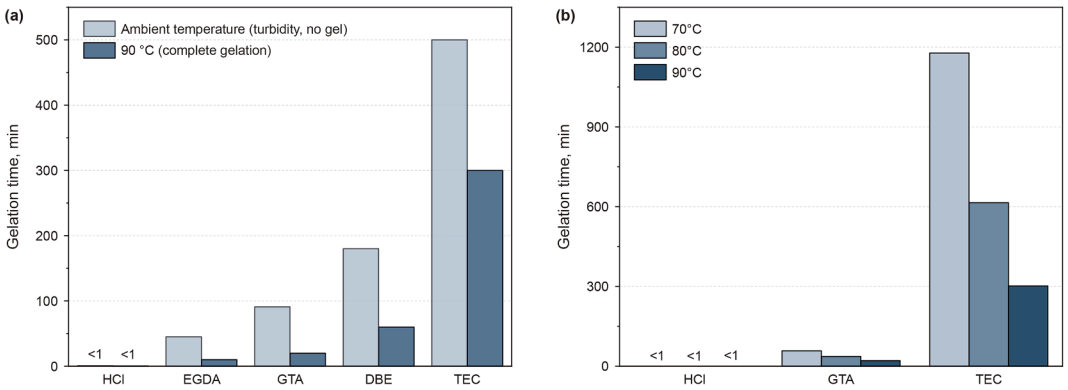


Fig. 2. Gelation kinetics of ester-triggered silicate systems. (**a**) Trigger screening at ambient temperature and 90 °C (TEC data measured at ambient temperature denote turbidity onset rather than rigid gelation). (**b**) Thermal-gating response at 70–90 °C, demonstrating the extended safe-injection window.

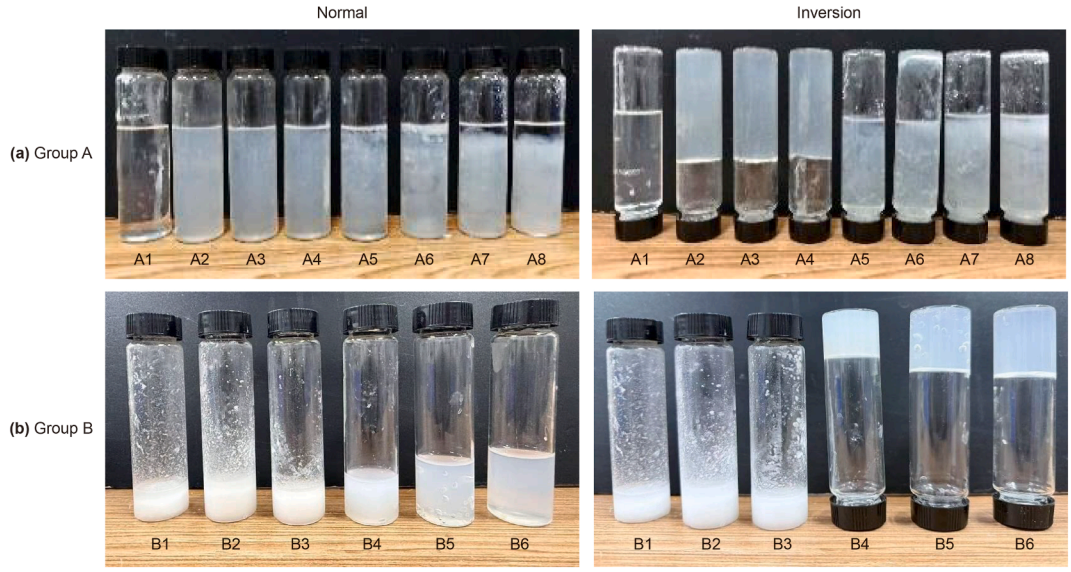


Fig. 3. Macroscopic phase transitions and structural integrity evaluations of the gel system via the visual bottle inversion method. (**a**) Effect of TEC/Na_2SiO_3 mass ratio at a fixed silicate concentration (2.5 wt%). (**b**) Effect of total reactant concentration at a fixed optimal TEC/Na_2SiO_3 mass ratio (2.0).

Table 1
Comprehensive formulation screening matrix: physicochemical parameters, macroscopic phase behaviour, and evaluations of the TEC-triggered silicate system under varied concentration gradients and mass ratios.

Group	Experimental variable	Na_2SiO_3, wt%	TEC, wt%	TEC/Na_2SiO_3 mass ratio	pH	Macroscopic behaviour	Evaluation
A1	Varied TEC concentration	2.50	1.25	0.5	12.2	Flowable solution	No gel
A2	Varied TEC concentration	2.50	2.50	1.0	11.7	Uniform gel formed	Gel
A3	Varied TEC concentration	2.50	3.75	1.5	11.4	Uniform gel formed	Gel
A4	Varied TEC concentration	2.50	5.00	2.0	11.0	Stable uniform gel formed	Gel, selected formulation
A5	Varied TEC concentration	2.50	6.25	2.5	10.6	No stable bulk gel	No stable gel
A6	Varied TEC concentration	2.50	7.50	3.0	10.1	Precipitation/phase separation	No uniform gel
A7	Varied TEC concentration	2.50	8.75	3.5	9.2	Precipitation/phase separation	No uniform gel
A8	Varied TEC concentration	2.50	10.00	4.0	8.4	Precipitation/phase separation	No uniform gel
B1	Varied total concentration at fixed ratio	7.50	15.00	2.0	—	Precipitation/phase separation	No uniform gel
B2	Varied total concentration at fixed ratio	6.25	12.50	2.0	—	Precipitation/phase separation	No uniform gel
B3	Varied total concentration at fixed ratio	5.00	10.00	2.0	—	Precipitation/phase separation	No uniform gel
B4	Varied total concentration at fixed ratio	3.75	7.50	2.0	10.9	Uniform gel formed	Gel
B5	Varied total concentration at fixed ratio	3.00	6.00	2.0	10.9	Uniform gel formed	Gel
B6	Varied total concentration at fixed ratio	2.50	5.00	2.0	11.0	Stable uniform gel formed	Gel, selected formulation

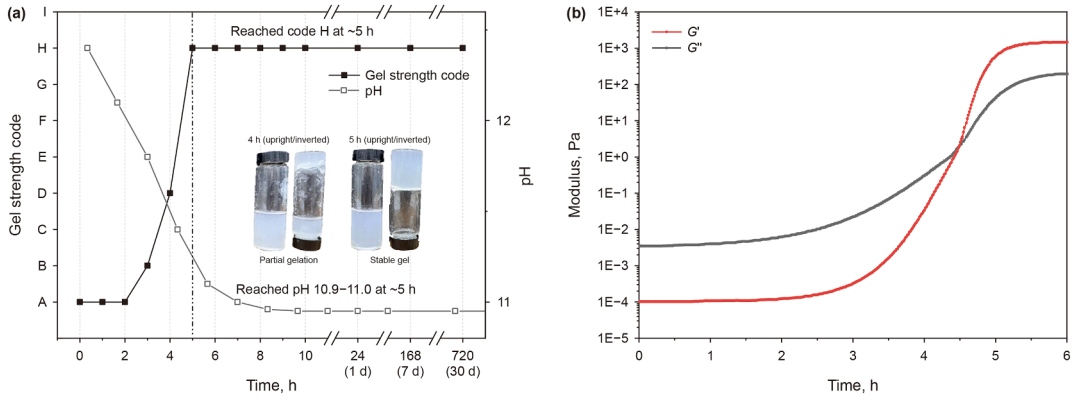


Fig. 4. Gelation behaviour and pH evolution of the sodium metasilicate–TEC system at 90 °C. (**a**) Time-dependent changes in gel strength code and pH during the gelation process. (**b**) Evolution of storage modulus G' and loss modulus G'' as a function of reaction time.

reflecting ongoing condensation of silicate species and the progressive formation of a continuous three-dimensional network.

Macroscopically, the system developed noticeable viscosity after 4 h, signaling the onset of gel-network formation, although it had not yet reached a stable, non-flowing state. By 5 h, however, the sample remained completely immobile upon vial inversion, confirming that effective gelation had been achieved and that a relatively stable gel network had formed. Long-term thermal aging tests were further conducted to evaluate the stability of the optimized gel system. As shown in Fig. 4(a), the gel maintained its structural integrity after prolonged exposure to elevated temperatures, demonstrating good thermal stability under the tested conditions. Thereafter, the gel strength remained consistently high, demonstrating that the optimized sodium metasilicate–TEC system not only provides a suitable delayed gelation time but also forms a highly stable gel structure.

To provide quantitative support for the proposed pH-triggered gelation mechanism, the pH evolution of the sodium metasilicate–TEC system was monitored at 90 °C. The initial pH was 12.4 due to the strong alkalinity of sodium metasilicate. With increasing reaction time, the pH gradually decreased to 12.1 after 1 h, 11.8 after 2 h, 11.4 after 3 h, 11.1 after 4 h, and 10.9 after 5 h. The gel state changed consistently with the pH decrease, evolving from a flowable solution to a slightly thickened state, viscous state, weak gel, and finally a complete non-flowing gel. These results indicate that TEC-induced gradual pH evolution plays a key role in triggering sodium metasilicate polycondensation and gel-network formation.

Time-dependent oscillatory rheological measurements were performed to quantitatively characterize the gelation process (Fig. 4(b)). The crossover of G' and G'' was defined as the rheological gel point, and the subsequent dominance of G' over G'' confirmed the formation of an elastic silicate gel network.

3.4. Mechanistic analysis of TEC-induced delayed gelation

To further elucidate the TEC-regulated gelation mechanism, the acid-source screening results (Fig. 2) were analyzed alongside the molecular schematic illustration in Fig. 5. This kinetic delay is proposed to be closely associated with the sterically hindered molecular architecture of TEC. Unlike simple short-chain esters (e.g., GTA) or direct HCl addition, the bulky citrate backbone and three ethyl ester groups of TEC reduce the accessibility of the ester carbonyl groups to nucleophilic attack by OH^- under alkaline conditions. This steric hindrance retards the hydrolysis rate, leading to gradual alkalinity consumption and progressive pH decrease rather than an abrupt pH collapse. Consequently, silicate polycondensation is shifted from rapid localized aggregation to a more controlled and homogeneous network-forming process. By coupling molecular-level hydrolysis kinetics with the macroscopic acidification trajectory, TEC allows the system to retain low viscosity during the induction period while enabling the subsequent formation of a high-strength three-dimensional silicate network at later stages.

3.5. Particle evolution during gelation and microstructural characteristics of the gel

To elucidate the structural evolution of the sodium metasilicate–TEC system, its dynamic particle-size distribution and microstructural features were characterized. As shown in Fig. 6, the particle size shifts progressively toward larger dimensions as the reaction proceeds. Initially, the distribution is centered around 10 nm, indicating the dominance of dispersed silicate oligomers. Over time, the peak shifts to larger particle sizes and broadens, reflecting continuous interparticle polycondensation and aggregation. Approaching the 5 h threshold, the system develops large-scale aggregates, corroborating the macroscopic gel-strength evolution. This dynamic sizing suggests that TEC-regulated gradual acidification suppresses abrupt local

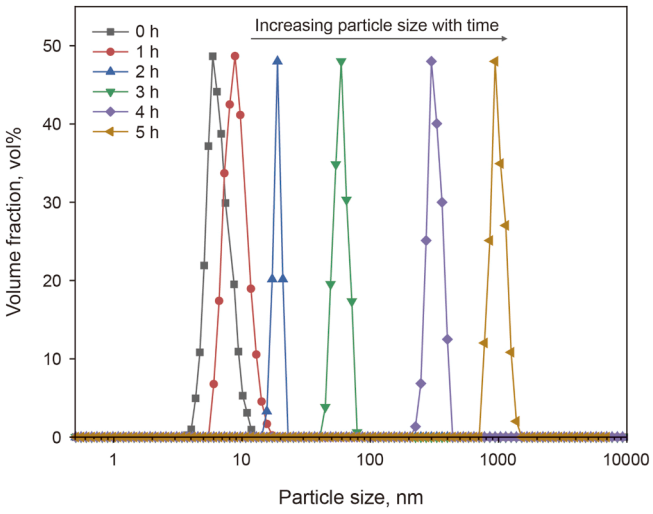


Fig. 6. Time-dependent evolution of particle size distribution during the gelation of the optimized sodium metasilicate–TEC system.

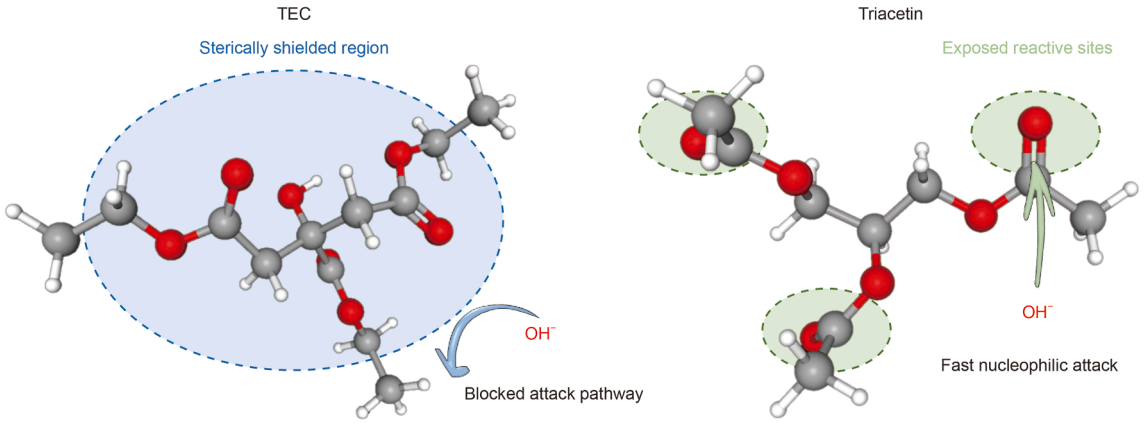


Fig. 5. Schematic illustration of the steric hindrance effect of TEC on alkaline hydrolysis.

flocculation and guides silicate species through a continuous structural reorganization process.

Fig. 7 further elucidates the micro-morphology of the optimized gel. The STEM images reveal aggregated structures in which nanoscale primary particles interconnect to form a continuous, cohesive three-dimensional network. This morphology indicates that the system forms an integrated inorganic skeleton rather than isolated precipitated clusters, consistent with the evolutionary pathway mapped by the DLS data.

To identify the elemental composition and spatial distribution within this skeleton, STEM-EDS mapping was performed (Fig. 8(a)). Si and O exhibit significant enrichment and co-localization across the particle regions, confirming the formation of a Si–O network structure. Na is also distributed within the particle regions, though its enrichment level is considerably lower, suggesting that it exists mainly as residual ions. Furthermore, the detection of B confirms the incorporation of borate species. As established in prior studies, nano-SiO_2 serves as a nucleation center to fortify the primary Si–O backbone, whereas borate ions provide reversible dynamic crosslinking points to mitigate inorganic brittleness (Sadeghnejad et al., 2022; Sheidaie et al., 2022). Therefore, while TEC acts as the primary kinetic trigger, these auxiliary components contribute to the macroscopic mechanical robustness of the final network. The quantitative EDS spectra (Fig. 8(b)) further verify this Si–O-dominated composition.

The aforementioned microstructural evolution and highly controlled pH trajectory confirm the robustness of the TEC-triggered network at the fundamental kinetic level. To validate whether this microscopic structural integrity can be successfully translated into effective deep conformance control under dynamic reservoir conditions, macroscopic core flooding experiments were systematically conducted.

3.6. Single-core plugging performance and pore-scale characterization

3.6.1. Evaluation of single-core flooding performance

To evaluate the plugging capacity of the silica gel system in porous media, single-core flooding experiments were conducted on high- and low-permeability cores, respectively; the results are illustrated in Figs. 9 and 10. Overall, both sets of experiments exhibited similar trends. During the initial water-flooding stage,

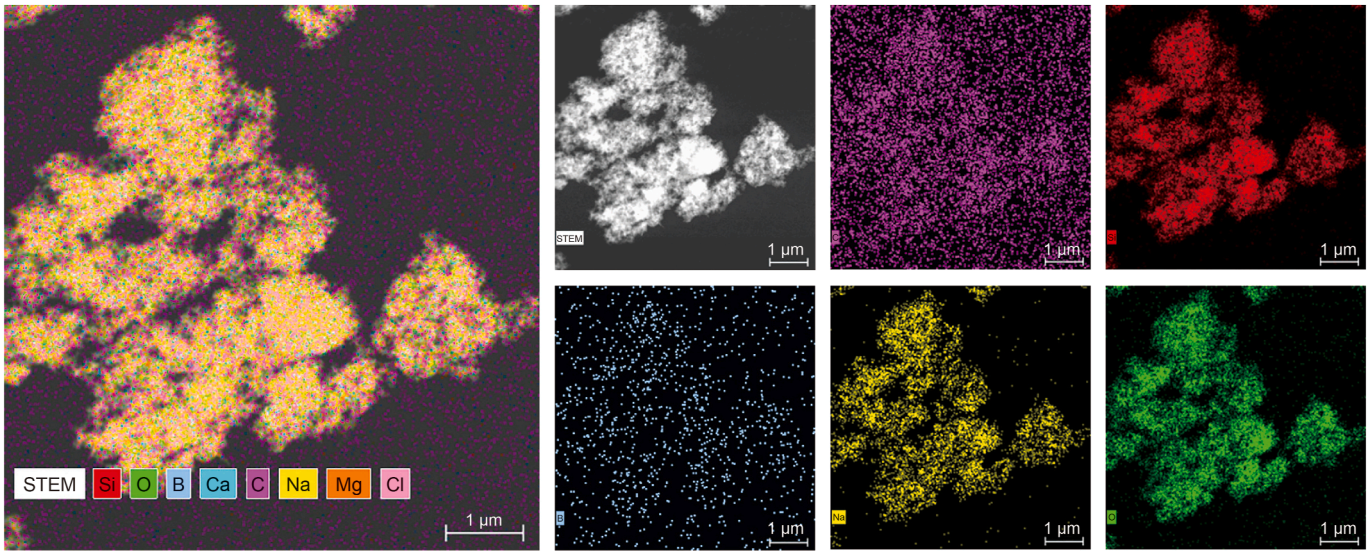


Fig. 7. STEM image and corresponding EDS elemental maps of the optimized sodium metasilicate–TEC gel particles.

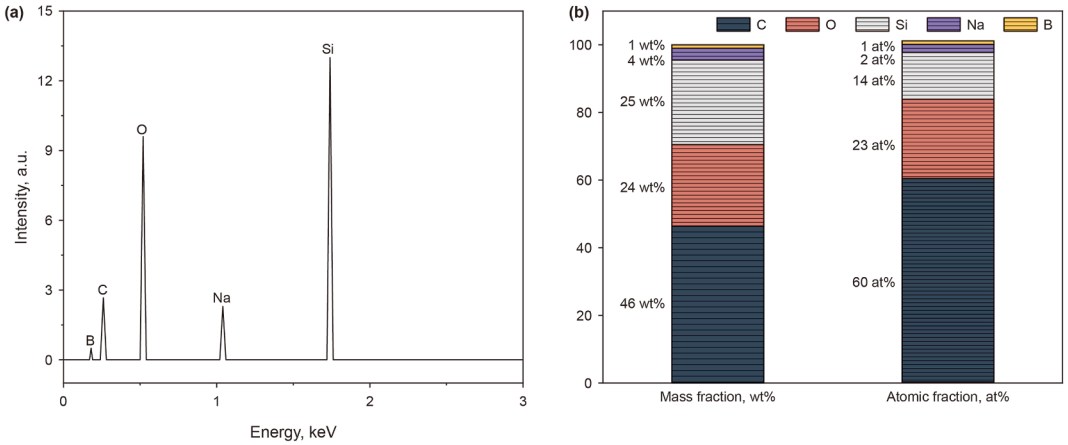


Fig. 8. EDS spectrum (**a**) and quantitative elemental composition (**b**) of the optimized sodium metasilicate–TEC gel.

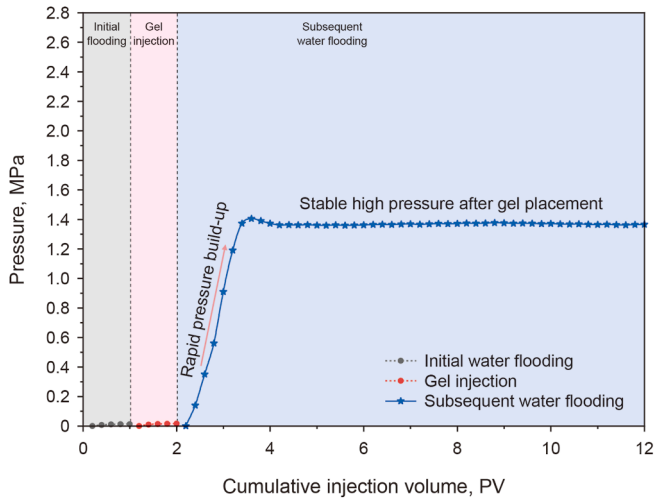


Fig. 9. Injection pressure profile during single-core flooding, gel injection, and subsequent water flooding in a high-permeability core.

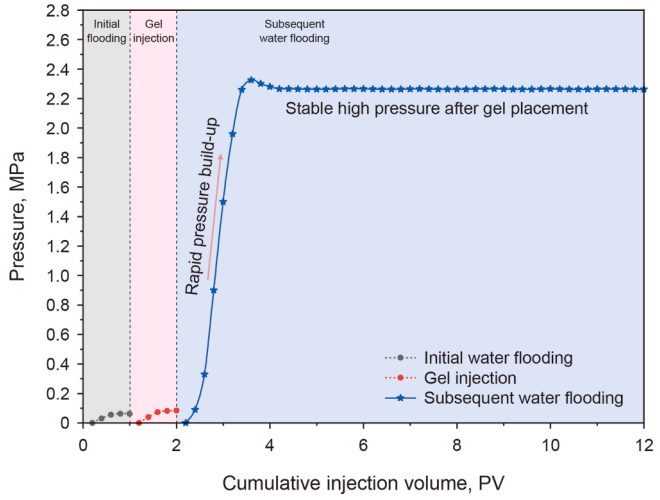


Fig. 10. Injection pressure profile during single-core flooding, gel injection, and subsequent water flooding in a low-permeability core.

the injection pressure remained low and stable, indicating that the fluid could smoothly pass through the core pores. During the gel system injection stage, only minor pressure fluctuations were observed, demonstrating that the system maintained good mobility and injectivity during the placement process. After aging, the subsequent water-flooding injection pressure rose sharply and remained at a high level, confirming that the gel system formed an effective plug within the core.

As illustrated in Fig. 9, the displacement pressure for the high-permeability core remained consistently low during both the initial water flooding and gel injection stages, with no significant pressure buildup observed. The initial displacement pressure was only 0.015 MPa, indicating that the gel system could smoothly penetrate the high-permeability pore channels. After 3 d of aging, the displacement pressure during the subsequent water flooding stage surged rapidly and stabilized at approximately 1.4 MPa, corresponding to a plugging efficiency of approximately 98%. This pronounced pressure buildup is consistent with the formation of a continuous silicate gel network, as supported by the microstructural observations in Section 3.5. Furthermore, throughout the subsequent 10 PV water flooding flush, the pressure curve exhibited no significant attenuation or severe fluctuations. This reflects that the gel formed a stable, high-resistance plugging structure within the high-permeability channels, demonstrating good resistance to subsequent water flushing.

As shown in Fig. 10, the low-permeability core also exhibited a distinct plugging response. Its initial water flooding pressure was approximately 0.10 MPa, which increased to 2.26 MPa after gelation and aging, achieving a plugging efficiency of 95%. Although the plugging efficiency of the low-permeability core was slightly lower than that of the high-permeability core, it developed a higher post-plugging pressure. This suggests that the gel system can be effectively retained within the low-permeability pore environment, establishing stable resistance. These findings validate that the sodium metasilicate–TEC system is not exclusively effective for high-permeability channels, but rather exhibits plugging capability across a broad range of permeability conditions.

Quantitative calculations indicate that the TEC-triggered gel exhibits strong mobility-control performance. Specifically, in the single-core tests, the water-flooding pressure differential in the high-permeability core surged from 0.015 to 1.4 MPa (corresponding to an RRF of 93.3 and a *PR* of 98.9%), whereas the *RRF* of the low-permeability core was 22.6 ($PR = 95.6\%$). In the heterogeneous parallel dual-core model, the comprehensive *RRF* also reached 85.7. These standardized data indicate that the gel network can maintain substantial flow resistance under water flushing. The difference in *RRF* values between the high- and low-permeability cores further suggests a preferential plugging tendency in heterogeneous porous media.

In summary, the TEC-triggered system maintains good injectivity during the initial placement phase and evolves into a high-resistance plugging structure post-gelation. This spatiotemporal synergy between delayed crosslinking and robust subsequent plugging is critical for enabling deep-formation penetration and ensuring long-term effective conformance control in heterogeneous reservoirs.

3.6.2. Post-plugging SEM characterization of the core

To further reveal the retention and deposition characteristics of the silica gel system on the pore surfaces, SEM and elemental composition analyses were performed on the carbonate core samples before and after treatment (Fig. 11). The original carbonate surface was generally smooth with high matrix continuity (Fig. 11(a)). Clear exposed pores and open channels were visible, indicating that the core maintained favorable seepage characteristics prior to treatment. In contrast, the surface morphology of the core underwent significant alterations after treatment (Fig. 11(b)). The originally smooth surface was covered by an adsorbed layer, with distinct granular aggregates appearing in localized areas. The surface roughness increased significantly, and some pore boundaries became blurred. These morphological changes indicate that during the displacement and aging processes, the gel system not only penetrated the pores but also formed a distinct deposition layer on the mineral surfaces, accompanied by particle aggregation and localized accumulation. Compared with the original surface, the presence of the attached layer and granular aggregates on the treated surface suggests that the plugging phase does not merely exist within the bulk fluid, but is capable of being retained and forming a stable covering structure on the pore walls and within throat regions. This deposition and aggregation reduce the effective pore throat size and increase flow resistance, thereby providing a microscopic basis for subsequent plugging and fluid diversion.

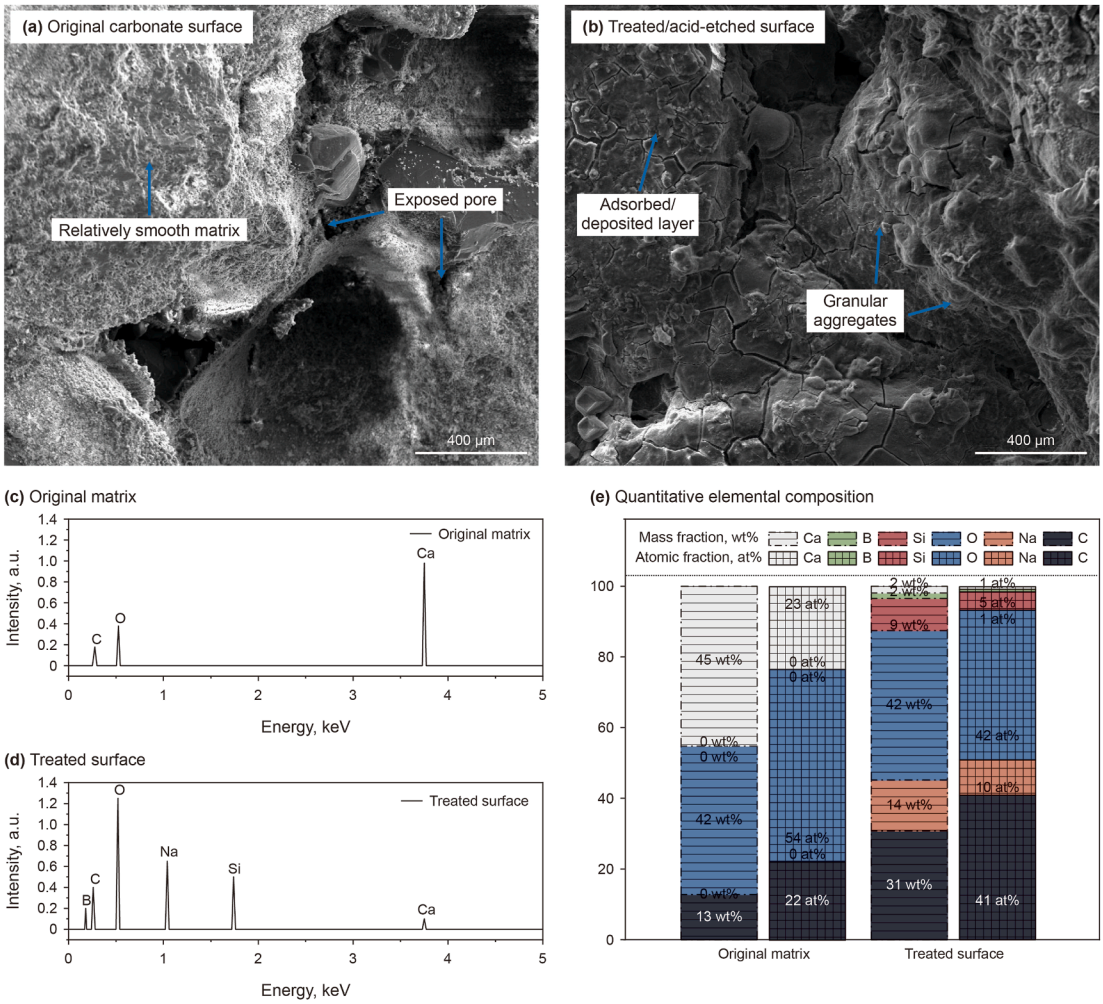


Fig. 11. SEM images (**a**, **b**) and elemental composition analysis (**c**–**e**) of the carbonate core surfaces before and after gel treatment.

As shown in the quantitative EDS elemental analysis (Fig. 11(c)–(e)), the original carbonate matrix was primarily composed of a high content of Ca (45 wt%) and contained no Si. After gel treatment, the detected Ca content decreased to approximately 2 wt%, while Si and Na increased to approximately 9 and 14 wt%, respectively. This change in elemental composition indicates the coverage of the carbonate surface by a silicate-rich gel phase.

3.6.3. NMR characterization of the single core

To further analyze the changes in pore fluid distribution before and after plugging, low-field NMR tests were conducted. As a non-destructive technique, NMR has been widely recognized for its ability to quantitatively characterize pore-scale fluid occurrence and plugging performance.

Fig. 12 shows the evolution of the T_2 relaxation time distributions for the low- and high-permeability cores,

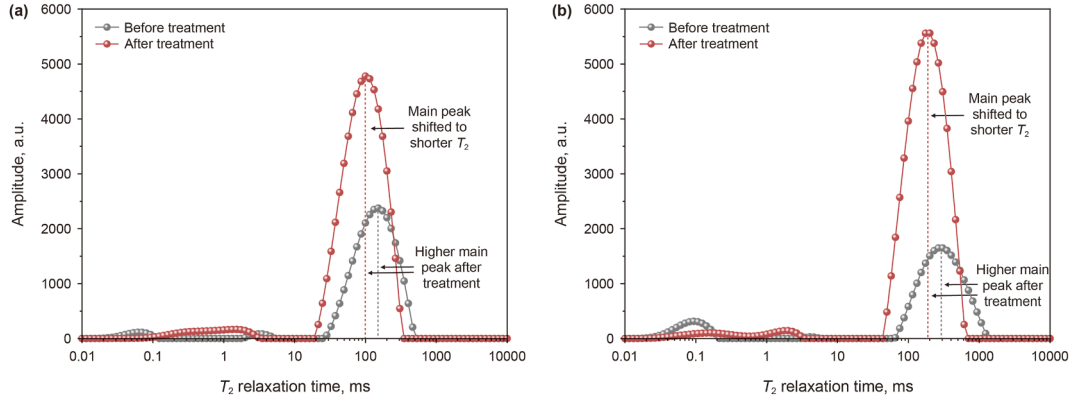


Fig. 12. Changes in T_2 relaxation time distributions of the single cores before and after gel treatment: (**a**) low-permeability core; (**b**) high-permeability core.

respectively, before and after gel treatment. After gel treatment, the primary T_2 peaks for both core types shifted significantly toward shorter relaxation times (leftward shift). Specifically, the primary peak of the high-permeability core shifted leftward from approximately 280 to 175 ms, and that of the low-permeability core shifted leftward from approximately 160 to 100 ms. This characteristic leftward shift indicates that the free water originally present in the large pore channels was converted into restricted bound water by the in-situ cross-linked silicate network. Simultaneously, the primary peak amplitudes of both cores showed a substantial increase. Specifically, the primary peak amplitude of the high-permeability core surged from approximately 2000 to 5500, and that of the low-permeability core jumped from approximately 2500 to 5000. This increase in signal intensity suggests enhanced retention of pore fluid associated with gel formation. These

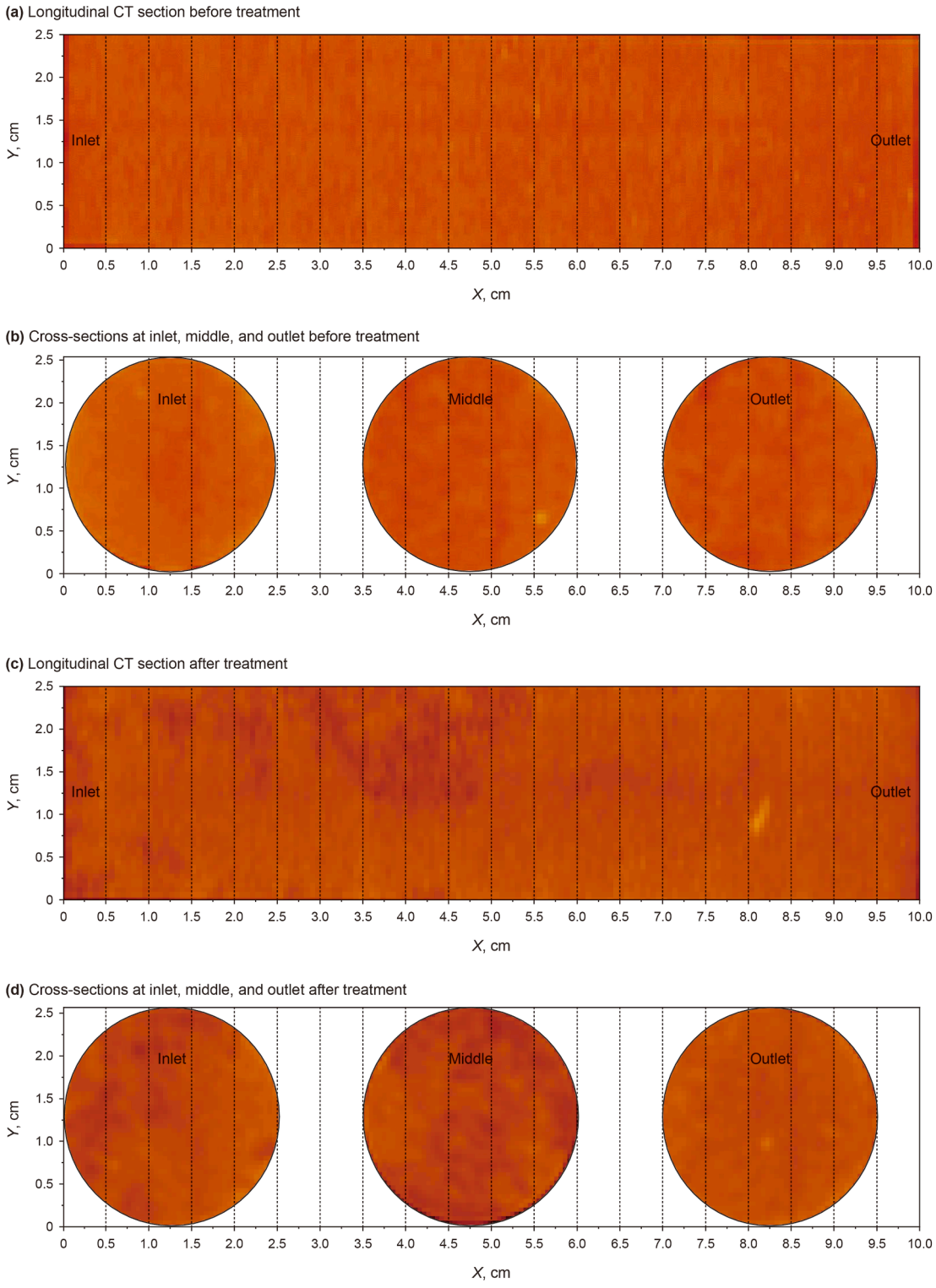


Fig. 13. Longitudinal and cross-sectional CT images of the low-permeability core before (**a**, **b**) and after (**c**, **d**) gel treatment in the single-core flooding experiment.

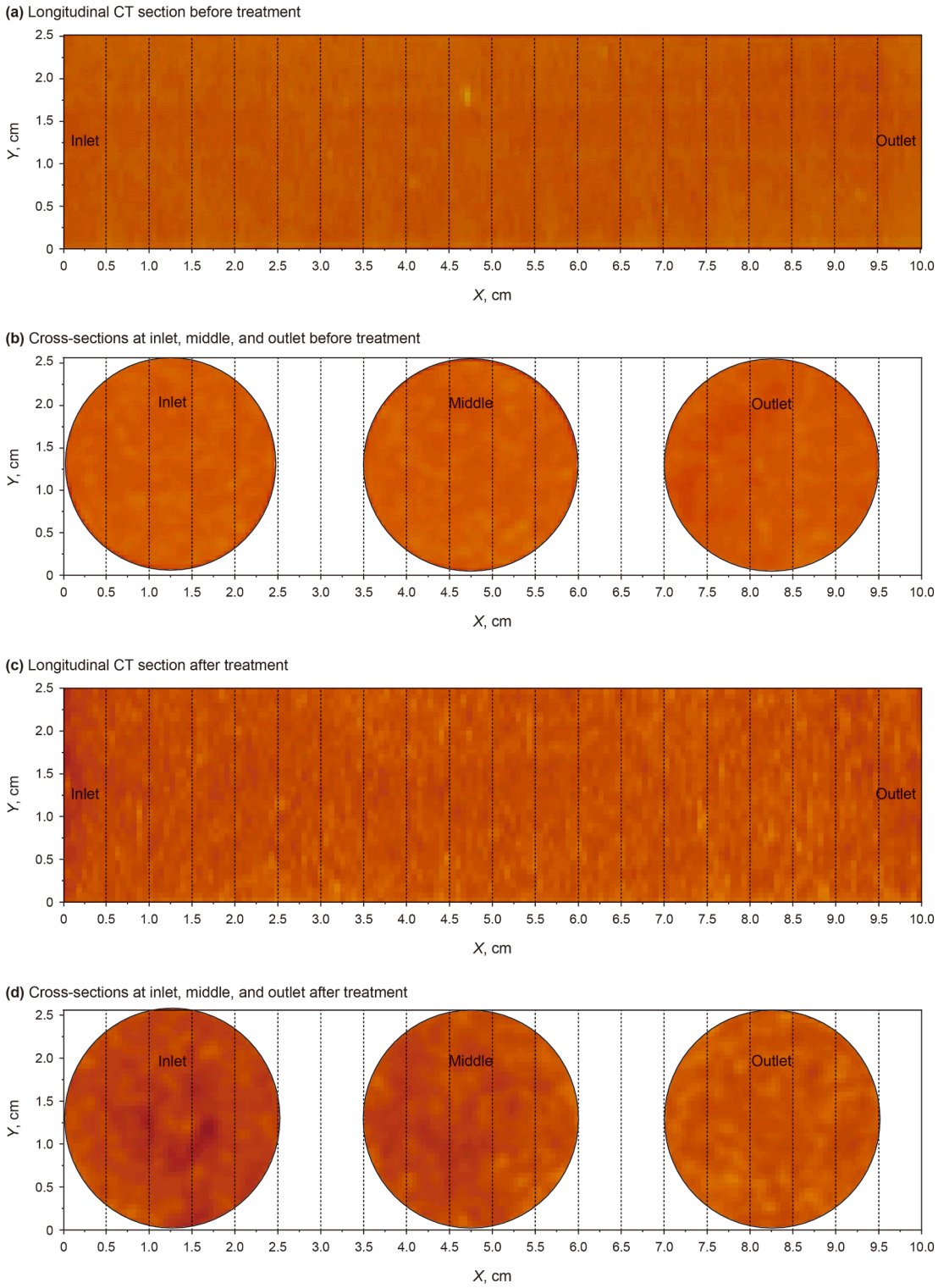


Fig. 14. Longitudinal and cross-sectional CT images of the high-permeability core before (**a**, **b**) and after (**c**, **d**) gel treatment in the single-core flooding experiment.

pore-scale micro-evolutions are consistent with the macroscopic displacement experiments—the conversion of free water to bound water in the microstructure and the large-volume filling of the gel perfectly correspond to the sharp increase in injection pressure and the process of effective structural plugging of the dominant flow pathways in the macroscopic experiments.

3.6.4. CT characterization of the single core

As shown in Figs. 13 and 14, CT scan results further validated the plugging behaviour from a spatial distribution perspective. Significant gel retention was observed within both high- and low-permeability cores after treatment. The scan images revealed that the gel was distributed throughout the entire core length rather than being restricted to the inlet face,

confirming the deep migration capability of the sodium metasilicate–TEC system.

This spatial evidence is highly consistent with the NMR findings. The preferential occupancy of the gel in large channels and high-flow regions effectively attenuated the fluid flow capacity and established stable resistance. The relatively homogeneous distribution of the gel phase within the core matrix indicates that the system can form an integral plugging structure after aging, providing the microstructural basis for its robust macroscopic performance.

In summary, the combined results from SEM, NMR, and CT analyses demonstrate that the sodium metasilicate–TEC system achieves comprehensive plugging across a range of permeabilities. The system not only exhibits a significant macroscopic pressure response but also induces extensive pore-scale channel obstruction and alters fluid occurrence states, supporting its deep-plugging capability.

3.7. Fluid diversion and selective plugging characterization in dual-core systems

3.7.1. Displacement pressure and flow distribution in dual-core flooding

To further evaluate the selective plugging and fluid diversion capabilities of the silica gel system in heterogeneous porous media, parallel dual-core flooding experiments were conducted. Fig. 15 illustrates the pressure profile during parallel dual-core flooding, whereas Fig. 16 presents the corresponding evolution of flow distribution between the high- and low-permeability cores. Overall, these findings provide direct evidence of both the plugging effect in the high-permeability channel and the subsequent redistribution of flow.

As shown in Fig. 15, during the initial water-flooding stage, the injection pressure in the parallel dual-core system remained low and stable at approximately 0.010 MPa, reflecting that the injected fluid preferentially flowed through the high-permeability core. During gel injection, the pressure increased only slightly to 0.014 MPa with no marked pressure buildup, demonstrating that the silica gel system retained excellent mobility and injectivity during placement. After 3 d of aging, the pressure during subsequent forward water flooding increased rapidly and stabilized at approximately 1.2 MPa (RRF = 85.7, PR = 98.8%). This parallel configuration demonstrates the fluid-diversion capability of the system: the gelant preferentially entered the high-permeability channel and formed a strong plug after aging, thereby redirecting subsequent injected water toward the previously unswept low-permeability core. This confirms that the gel system formed an effective and stable plugging structure within the parallel cores, particularly within the dominant flow channel.

In accordance with the pressure response, Fig. 16 shows the evolution of flow partitioning between the high- and low-permeability cores. During the initial water-flooding stage, the flow ratio was approximately 9:1, verifying that a pronounced preferential flow path was established. During gel injection, this flow ratio remained essentially unchanged, further indicating that the gel system preferentially entered the high-permeability channel with the bulk fluid without premature plugging. After aging, however, the flow ratio shifted markedly from 9:1 to 3:7 during forward water flooding, signaling that flow through the high-permeability core was strongly suppressed and that a greater fraction of the injected fluid was redirected into the low-permeability core. It can be deduced from this behaviour that the silica gel system forms an effective plug in the high-permeability channel, forcing subsequent fluid into the previously under-swept regions. This selective placement and diversion behaviour are consistent with the delayed gelation kinetics discussed in Section 3.3, which allow the gelant to remain mobile during placement before in-situ network formation.

Furthermore, during the reverse-flooding stage, Fig. 15 shows that the flooding pressure decreased markedly from 1.2 to 0.12 MPa, suggesting substantial pressure release. However, Fig. 16 reveals that the flow ratio shifted further to 1:9 under these conditions, confirming that the low-permeability core had become the dominant flow pathway. This result indicates that, although reverse flooding reduced the overall pressure drop, the plugging structure within the high-permeability channel remained intact. The high-permeability core did not re-emerge as the dominant path; instead, a more pronounced flow-diversion effect was observed.

This sharp decrease in injection pressure during reverse flooding can be attributed to the altered flow boundary conditions and the asymmetric distribution of the gel plug. During forward placement, the gel predominantly invaded the inlet

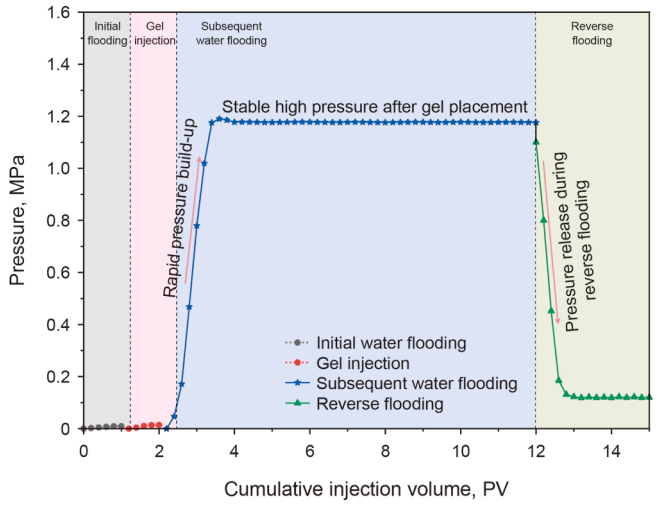


Fig. 15. Injection pressure profile during dual-core flooding, gel injection, subsequent water flooding, and reverse flooding.

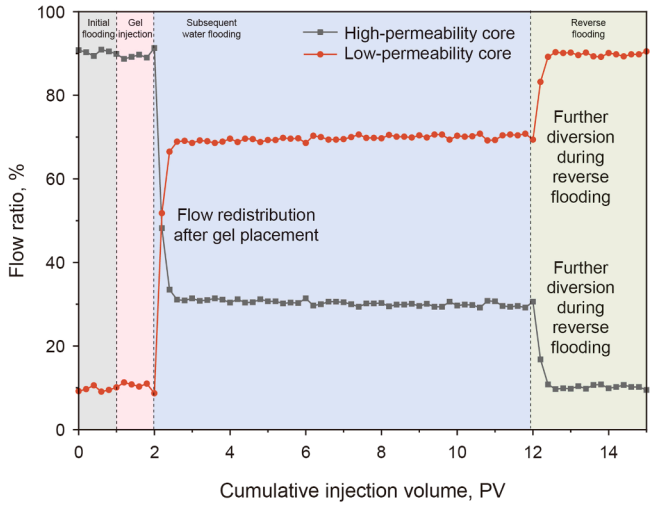


Fig. 16. Flow redistribution between the high- and low-permeability cores during dual-core displacement.

region of the high-permeability core, forming a high-resistance barrier. Under reverse flow, the water entered from the outlet. Since the low-permeability core suffered minimal gel invasion, it provided a highly conductive pathway in the reverse direction. The pressure dropped to approximately 0.12 MPa—which matched the inherent baseline pressure of the undamaged low-permeability core—because the fluid bypassed the forward-facing gel plug. The 1:9 flow ratio further corroborates that the gel plug remained structurally intact against reverse erosion, effectively maintaining the newly established fluid diversion.

Taken together, the pressure profiles and flow-distribution results demonstrate that the developed silica gel system possesses both strong selective plugging capability and sustained flow-diversion performance. Even under reverse-flooding conditions, the system continues to suppress flow through the high-permeability channel, indicating robust stability and resistance to erosive flushing.

3.7.2. NMR characterization of the dual-core system

To further clarify the selective entry behaviour of the gel within the high- and low-permeability cores under dual-core conditions, NMR measurements were performed separately on both cores after flooding. The results revealed a distinct contrast in the T_2 spectra between the two core types (Fig. 17).

For the high-permeability core (Fig. 17(b)), after gel treatment, the amplitude of the primary T_2 peak decreased significantly, demonstrating a marked reduction in the volume of movable fluid. Simultaneously, the primary peak shifted from approximately 300 to 200 ms. This leftward shift confirms that the gel preferentially occupied the larger pore channels and dominant flow pathways, effectively reducing the effective pore radii and altering the pore-scale fluid distribution. Conversely, the low-permeability core (Fig. 17(a)) exhibited negligible alterations in its T_2 profile, indicating an absence of substantial internal gel crosslinking.

These results indicate that, under parallel dual-core conditions, the sodium metasilicate–TEC system exhibits pronounced selective-entry behaviour: it predominantly invaded the high-permeability core to form an effective plug, while its penetration into the low-permeability matrix remained highly limited. This micro-scale validation is consistent with the redistribution of the flow ratio from 9:1 to 1:9, confirming that the observed flow diversion arose primarily from the obstruction of high-permeability channels rather than unintended formation damage to the low-permeability core.

3.7.3. CT characterization of the dual-core system

CT results further validated the distinct distribution of the gel within the heterogeneous system. As shown in Fig. 18, the CT images of the high-permeability core revealed extensive gel filling along its longitudinal axis, confirming that the gel had formed a relatively complete deep plug. In contrast, the CT images of the low-permeability core (Fig. 19) showed that the gel was concentrated primarily near the inlet face, with retention restricted to approximately the first 10% of the core length and no significant penetration into deeper regions.

These spatial observations demonstrate that during parallel dual-core flooding, the gel system partitioned unevenly. It migrated preferentially through the high-permeability channel, forming the principal plugging structure. The increased flow through the low-permeability core during subsequent flooding was not due to extensive gel filling within that core itself but was instead a direct consequence of the marked reduction in flow capacity within the high-permeability core. This reduction successfully forced the injected fluid to divert into the previously bypassed low-permeability zones.

3.8. Field applicability, methodological limitations, and future perspectives

3.8.1. Field applicability

To evaluate the reservoir field applicability of the system, the physicochemical interference of formation salinity and divalent cations (Ca^{2+}, Mg^{2+}), and inherent rock pH buffering capacities must be addressed. Divalent cations in high-salinity formation water may accelerate silicate aggregation or precipitation, which can reduce injectivity and narrow the placement window. In the TEC-triggered system, citrate-derived species generated during ester hydrolysis may complex Ca^{2+} and Mg^{2+}, potentially reducing cation-induced precipitation (Hashemi et al., 2023). This effect may contribute to maintaining the induction period required for deep placement, although its extent under specific reservoir brines requires further verification.

In addition to ionic interference, the inherent pH buffering capacity of reactive rock minerals (particularly carbonates) poses a critical challenge by consuming H^+ during the gelation process. The optimized TEC formulation provides a gradual acidification capacity through ester hydrolysis, which can partially compensate for alkalinity buffering or acid consumption by reactive minerals.

From an operational perspective, a compatible pre-flush may be required before gelant injection to reduce the influence of

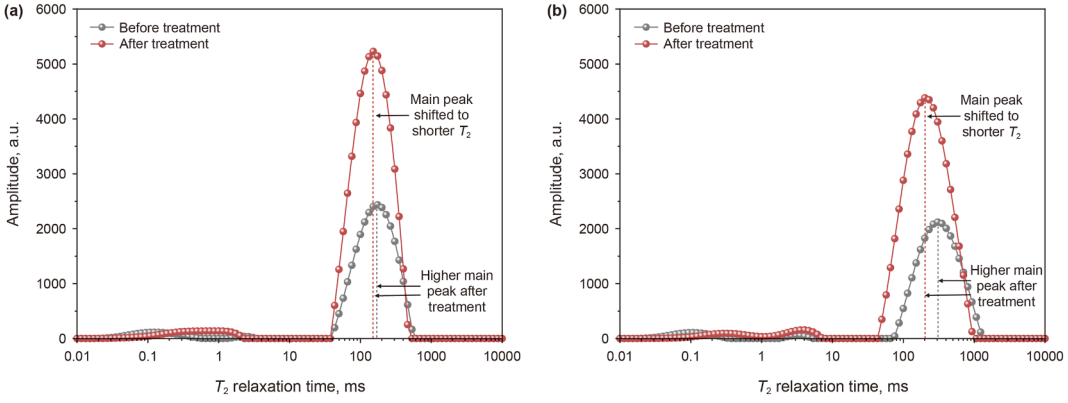


Fig. 17. T_2 relaxation time distributions before and after gel treatment in the parallel dual-core experiment: (**a**) low-permeability core; (**b**) high-permeability core.

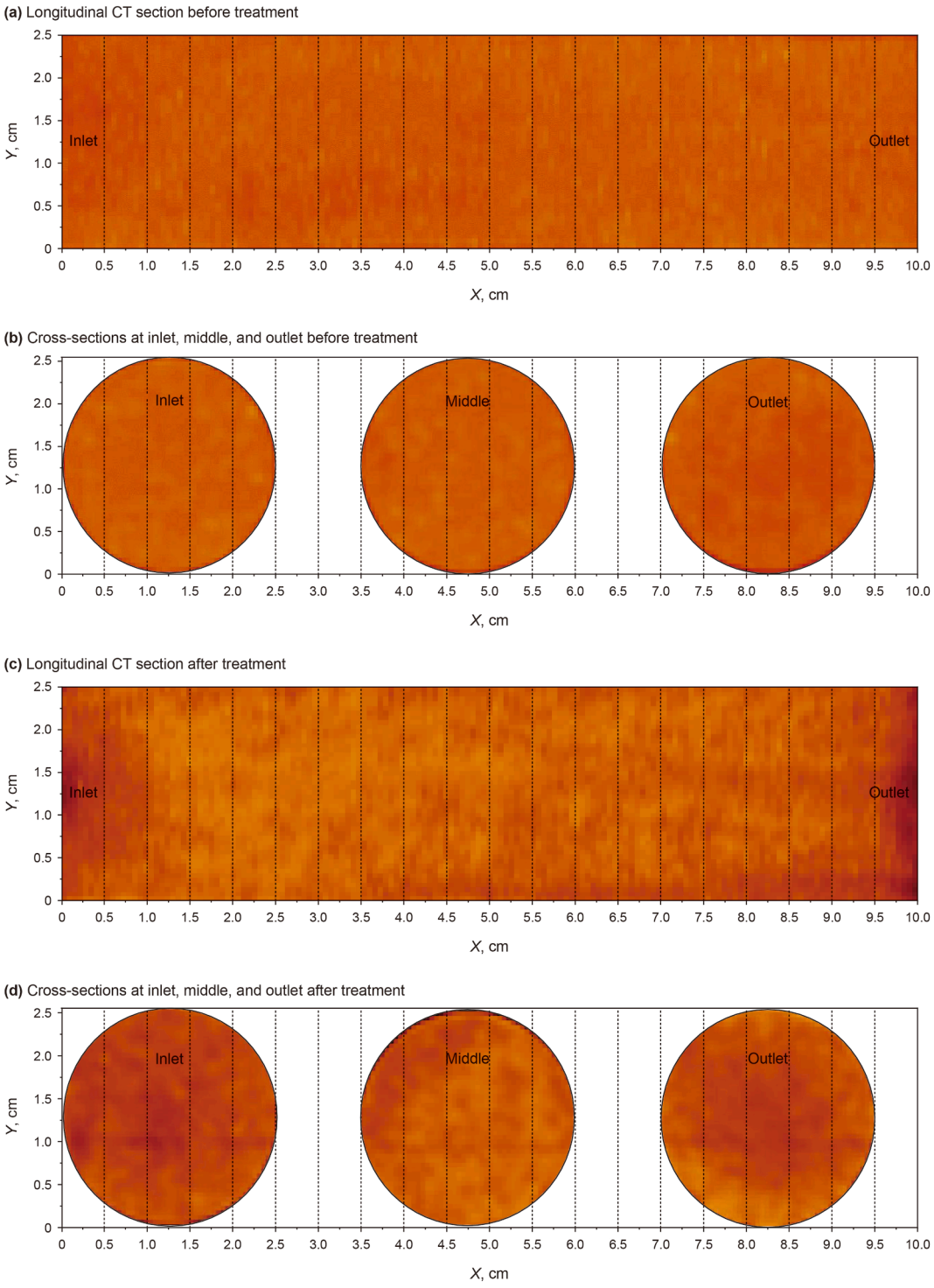


Fig. 18. Longitudinal and cross-sectional CT images of the high-permeability core before (**a**, **b**) and after (**c**, **d**) gel treatment in the parallel dual-core plugging experiment.

highly saline or strongly buffered formation water near the wellbore. Such a pre-flush can help establish a more controlled aqueous environment for gelant placement. In deeper target zones, residual ions or mineral buffering may still influence local silicate condensation and gel retention. These interactions could either promote local plugging or disturb gelation, depending on the specific brine composition and rock mineralogy; therefore, they should be evaluated under reservoir-specific conditions before field deployment.

It is critical to distinguish the operational time window of the inorganic silicate system from conventional organic polymer standards. Unlike polymer crosslinking, which relies on molecular entanglement and typically exhibits high initial viscosity, the silicate condensation mechanism ensures a water-like, ultra-low

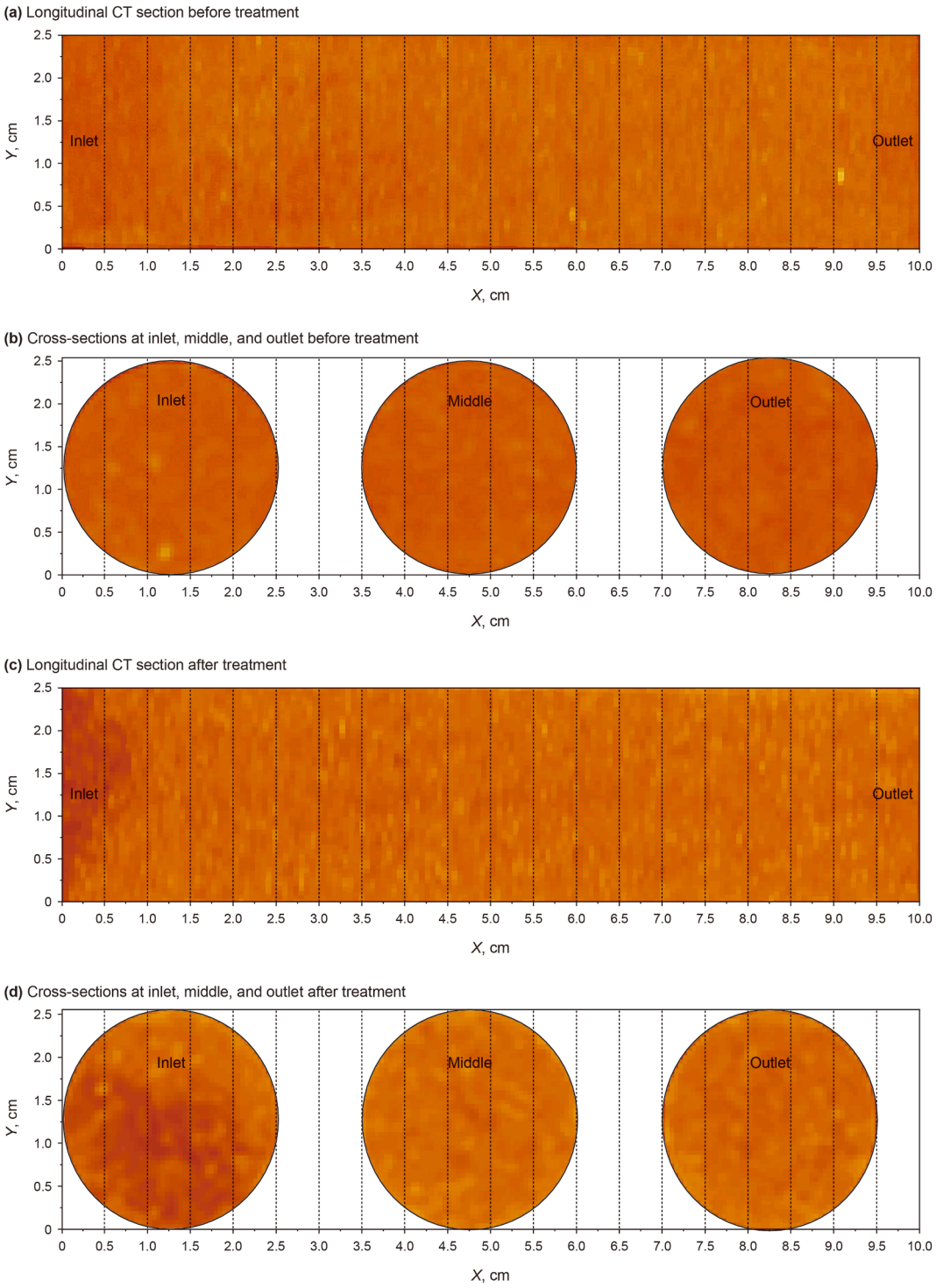


Fig. 19. Longitudinal and cross-sectional CT images of the low-permeability core before (**a**, **b**) and after (**c**, **d**) gel treatment in the parallel dual-core plugging experiment.

viscosity throughout the injection period, fundamentally reducing hydraulic resistance during injection. The 5 h gelation time measured at 90 °C should therefore be interpreted as a static laboratory gelation time under reservoir-temperature conditions, rather than as a universal pumping-time limit. In field operations, the actual placement window may be affected by the temperature profile from the surface to the target formation, injection rate, wellbore residence time, and heat transfer. The temperature-dependent gelation observed in this study suggests that lower temperatures during early placement may further delay gelation, whereas exposure to the target reservoir temperature can promote subsequent network formation.

It should be noted that the volume stability of the latent acid–sodium metasilicate system investigated here differs from that of conventional polymer gels. In typical crosslinked polymer gels, volume changes are governed by swelling equilibrium, which is highly sensitive to polymer–solvent interactions, osmotic pressure, and network elasticity (Bashir et al., 2020). In contrast, the

present system forms an inorganic silicate network through acid-induced pH regulation and polycondensation (Brinker and Scherer, 1985; Matinfar and Nychka, 2023). This difference arises because polymer gels contain flexible, solvated polymer chains that can expand or contract in response to osmotic pressure and solvent quality, whereas the present inorganic gel is mainly composed of condensed Si–O–Si networks with limited segmental mobility. Therefore, the latent acid structure primarily regulates hydrolysis kinetics and mechanical development rather than volumetric expansion. Consistent with the 30-d thermal aging observations (Fig. 4(a)), the optimized TEC-regulated gel maintained good structural integrity at 90 °C without noticeable syneresis or collapse. A comprehensive evaluation of changes of gel volumes across broader salinity, pH, and temperature ranges requires a separate systematic study and should be addressed in future work.

3.8.2. Methodological limitations

The conclusions currently drawn in this study are primarily based on single-core and dual-core physical models under controlled boundary conditions. To achieve methodological variable isolation, we adopted the parallel dual-core model to evaluate the relative selective plugging and flow diversion dynamics at the pore scale. However, actual strongly heterogeneous reservoirs possess significantly higher geometric and physical complexities, including extreme permeability contrasts, fracture-matrix dual-porosity systems, and multi-layer crossflow dynamics. Therefore, the current core-flooding results should be regarded strictly as a mechanistic proof of concept for fluid diversion, rather than a direct definition of the operational limits for field engineering.

3.8.3. Future perspectives

To comprehensively establish the field-scale applicability of this system, future research should focus on fluid migration and long-term dynamic evolution in highly complex media. Subsequent experimental studies could utilize large-scale three-dimensional heterogeneous physical models and fracture-matrix dual-porosity media to systematically evaluate plugging effects under ultra-wide permeability contrasts. Simultaneously, combining these experimental results with numerical simulations under reservoir conditions to optimize slug sizes and injection parameters will help bridge the gap between laboratory mechanisms and macroscopic reservoir engineering applications.

In addition, while this study confirms the structural robustness of the TEC-triggered system during the critical gelation and initial deployment phases, future work will focus on evaluating long-term stability under representative brine, temperature, pressure, and flow conditions. Establishing this long-term performance profile is important for assessing the sustained conformance control capacities of the gel network under reservoir-relevant conditions.

4. Conclusions

A delayed sodium metasilicate gel system, regulated by a latent acid, was developed in this study, and its gelation behaviour, structural evolution, and plugging performance were systematically investigated. The main conclusions are as follows.

(1) Latent acids improved the controllability of gelation in the sodium metasilicate system. Systematic comparisons among direct acidification (HCl), short-chain esters (GTA), and sterically hindered esters (TEC) demonstrated that the molecular structure of the acid source strongly influenced the hydrolysis pathway. Compared with direct acidification by HCl or rapid hydrolysis of GTA, the bulky structure of TEC provided a wider and more controllable delayed-gelation window. Based on this, an optimized silica gel system composed of sodium metasilicate, TEC, nano-SiO_2, and borax was developed, achieving an effective gelation time of approximately 5 h at 90 °C and demonstrating good 30-d thermal stability without syneresis.

(2) TEC regulated the gelation kinetics through controlled acid release. Due to the steric hindrance associated with the TEC molecular structure, both its hydrolysis and acid-release processes were slowed, resulting in a more gradual decrease in pH and a shift in silicate polycondensation from a rapid, abrupt process to a progressive network-forming process. Particle size analysis showed a continuous shift in the distribution toward larger sizes with increasing reaction time, while TEM and elemental analysis further confirmed the eventual formation of a continuous Si–O-rich gel network.

(3) The optimized silica gel system exhibited effective plugging performance in cores with different permeabilities. In high-permeability single cores, the injection pressure increased from 0.015 to approximately 1.4 MPa, corresponding to a plugging efficiency of approximately 98%. In low-permeability single cores, the pressure increased from 0.10 to 2.26 MPa, with a plugging efficiency of 95%. In both cases, the pressure remained stable during subsequent flushing with 10 pore volumes (PV) of water, indicating stable plugging performance under continued water flooding.

(4) Parallel dual-core experiments demonstrated that the system possessed selective plugging and flow-diversion capabilities. During parallel dual-core flooding, the system maintained good injectivity during placement. After 3 d of aging, the pressure during subsequent water flooding rose to approximately 1.2 MPa, corresponding to an overall plugging efficiency of approximately 98%. Concurrently, the flow ratio between the high- and low-permeability cores changed from 9:1 during initial water flooding to 3:7 after aging, and further to 1:9 after reverse flooding, indicating that the gel preferentially entered and plugged the high-permeability channel, thereby redirecting subsequent flow toward the low-permeability region.

(5) Multiscale characterization revealed both overall plugging and selective plugging behaviour. In single-core experiments, NMR measurements and CT images showed that the system achieved substantial pore-scale plugging. By contrast, under dual-core conditions, only the high-permeability core exhibited a clear shift in the primary T_2 peak (from 300 to 200 ms), while the low-permeability core remained essentially unchanged. CT results further showed that the high-permeability core was extensively filled with gel, whereas the low-permeability core contained only a minor amount of gel within the proximal 10% of the inlet section. These observations demonstrated that the system preferentially plugged the high-permeability channel while preserving the subsequent sweep capacity of the low-permeability region.

Taken together, this study establishes a clear relationship among latent-acid structure, acid-release behaviour, gel-network formation, and plugging/flow-diversion performance. These results demonstrate that latent-acid regulation is an effective method for achieving delayed gelation and selective plugging in sodium metasilicate systems, providing an experimental basis for the design of controllable inorganic gel systems.

CRediT authorship contribution statement

Kun Zhang: Writing – review & editing, Writing – original draft, Formal analysis, Data curation, Conceptualization. **Er-Dong Yao:**

Validation, Methodology, Funding acquisition. **Yi-Peng Zhong:** Visualization. **Lin Tan:** Data curation. **Jia-Wei Sheng:** Investigation. **Li-Li Wang:** Resources. **Fu-Jian Zhou:** Supervision, Project administration, Funding acquisition.

Declaration of competing interest

The authors declare that they have no known competing financial interests or personal relationships that could have appeared to influence the work reported in this study.

Acknowledgements

This research was funded by the National Science and Technology Major Projects of China (Grant No. 2025ZD1401406), the Key Program of the Joint Fund of the National Natural Science Foundation of China (Grant Nos. U23B2084, U25D9018) and the Innovative Research Group Project of the National Natural Science Foundation of China (Grant No. 52421002).

References

Ahmed, N.B., Ronsin, O., Mouton, L., Sicard, C., Yepremian, C., Baumberger, T., et al., 2017. The physics and chemistry of silica-in-silicates nanocomposite hydrogels and their phycocompatibility. J. Mater. Chem. B 5 (16), 2931–2940. https://doi.org/10.1039/c7tb00341b.

Bashir, S., Hina, M., Iqbal, J., Rajpar, A.H., Mujtaba, M.A., Alghamdi, N.A., et al., 2020. Fundamental concepts of hydrogels: Synthesis, properties, and their applications. Polymers 12 (11), 2702. https://doi.org/10.3390/polym12112702.

Brinker, C.J., 1988. Hydrolysis and condensation of silicates: Eeffects on structure. J. Non-Cryst. Solids 100 (1–3), 31–50. https://doi.org/10.1016/0022-3093(88)90005-1.

Brinker, C.J., Scherer, G.W., 1985. Sol → gel → glass: I. Gelation and gel structure. J. Non-Cryst. Solids 70 (3), 301–322. https://doi.org/10.1016/0022-3093(85)90103-6.

Harman, C., McDonald, M., Short, P., Ott, W., 2021. Silica gel fracturing fluids an alternative to guar systems that allows the use of West Texas produced water. In: SPE Hydraulic Fracturing Technology Conference and Exhibition. https://doi.org/10.2118/204144-MS.

Hashemi, S.J., Hormozi, F., Mokhtari, R., 2023. Controlling the gelation time of sodium silicate gelants for fluid management in hydrocarbon reservoirs. Fuel 341, 127645. https://doi.org/10.1016/j.fuel.2023.127645.

Jesionowski, T., 2002. Characterization of silicas precipitated from solution of sodium metasilicate and hydrochloric acid in emulsion medium. Powder Technol. 127 (1), 56–65. https://doi.org/10.1016/S0032-5910(02)00093-1.

Jurinak, J.J., Summers, L.E., 1991. Oilfield applications of colloidal silica gel. SPE Prod. Eng. 6 (4), 406–412. https://doi.org/10.2118/18505-PA.

Katoueizadeh, E., Rasouli, M., Zebarjad, S.M., 2020. A comprehensive study on the gelation process of silica gels from sodium silicate. J. Mater. Res. Technol. 9 (5), 10157–10165. https://doi.org/10.1016/j.jmrt.2020.07.020.

Larrondo, L.E., Urness, C.M., Milosz, G.M., 1985. Laboratory evaluation of sodium hydroxide, sodium orthosilicate, and sodium metasilicate as alkaline flooding agents for a Western Canada reservoir. In: SPE Oilfield and Geothermal Chemistry Symposium. https://doi.org/10.2118/13577-MS.

Liu, S., Ott, W.K., 2020. Sodium silicate applications in oil, gas & geothermal well operations. J. Pet. Sci. Eng. 195, 107693. https://doi.org/10.1016/j.petrol.2020.107693.

Matinfar, M., Nychka, J.A., 2023. A review of sodium silicate solutions: Structure, gelation, and syneresis. Adv. Colloid Interface Sci. 322, 103036. https://doi.org/10.1016/j.cis.2023.103036.

Matinfar, M., Nychka, J.A., 2024. Process mapping of the sol–gel transition in acid-initiated sodium silicate solutions. Gels 10 (10), 673. https://doi.org/10.3390/gels10100673.

Nasr-El-Din, H.A., Taylor, K.C., 2005. Evaluation of sodium silicate/urea gels used for water shut-off treatments. J. Pet. Sci. Eng. 48 (3–4), 141–160. https://doi.org/10.1016/j.petrol.2005.06.010.

Ng, S.Y., Shen, H.R., Lopez, E., Zherebin, Y., Barr, J., Schacht, E., et al., 2000. Development of a poly(ortho ester) prototype with a latent acid in the polymer backbone for 5-fluorouracil delivery. J. Contr. Release 65 (3), 367–374. https://doi.org/10.1016/S0168-3659(99)00218-7.

Obut, A., Girgin, İ., 2006. Preparation of sodium borosilicates using sodium silicate and boric acid. J. Sol. Gel Sci. Technol. 39 (2), 79–83. https://doi.org/10.1007/s10971-006-8974-6.

Pham, L.T., Hatzignatiou, D.G., 2016. Rheological evaluation of a sodium silicate gel system for water management in mature, naturally-fractured oilfields. J. Pet. Sci. Eng. 138, 218–233. https://doi.org/10.1016/j.petrol.2015.11.039.

Quang, D.V., Kim, J.-K., Park, J.-K., Park, S.-H., Elineema, G., Sarawade, P.B., et al., 2012. Effect of the gelation on the properties of precipitated silica powder produced by acidizing sodium silicate solution at the pilot scale. Chem. Eng. J. 209, 531–536. https://doi.org/10.1016/j.cej.2012.08.028.

Sadeghnejad, S., Ashrafizadeh, M., Nourani, M., 2022. Improved oil recovery by gel technology: Water shutoff and conformance control. In: Chemical Methods. Gulf Professional Publishing, Oxford, pp. 249–312. https://doi.org/10.1016/B978-0-12-821931-7.00001-8.

Sheidaie, A., Fahimpour, J., Sharifi, M., 2022. Experimental investigation of low-concentrated nanocomposite polymer gels for water shutoff treatment under reservoir conditions. SPE J. 27 (4), 2390–2407. https://doi.org/10.2118/209604-PA.

Sydansk, R.D., Argabright, P.A., 1987. Conformance Improvement in a Subterranean hydrocarbon-bearing Formation Using a Polymer Gel. US Patent US4683949A.

Wu, Q.-H., Ge, J.-J., Ding, L., Zhang, G.-C., 2023. Unlocking the potentials of gel conformance for water shutoff in fractured reservoirs: Favorable attributes of the double network gel for enhancing oil recovery. Pet. Sci. 20 (2), 1005–1017. https://doi.org/10.1016/j.petsci.2022.10.018.

Zhu, D.-Y., Deng, Z.-H., Chen, S.-W., 2021. A review of nuclear magnetic resonance (NMR) technology applied in the characterization of polymer gels for petroleum reservoir conformance control. Pet. Sci. 18 (6), 1760–1775. https://doi.org/10.1016/j.petsci.2021.09.008.